# Supporting Information

# Real-Time Studies of Iron Oxalate-Mediated Oxidation of Glycolaldehyde as a Model for Photochemical Aging of Aqueous Tropospheric Aerosols

*Daniel A. Thomas*[†,⊥], *Matthew M. Coggon*[‡,⊥,¶], *Hanna Lignell*[‡,§], *Katherine A. Schilling*[‡,‖], *Xuan Zhang*[§], *Rebecca H. Schwantes*[§], *Richard C. Flagan*[‡,§], *John H. Seinfeld*[‡,§], *and J. L. Beauchamp*[†,*]

[†]Arthur Amos Noyes Laboratory of Chemical Physics, California Institute of Technology, Pasadena, CA, 91125, USA

[‡]Division of Chemistry and Chemical Engineering, California Institute of Technology, Pasadena, CA, 91125, USA

[§] Environmental Science and Engineering, California Institute of Technology, Pasadena, CA, 91125, USA

*To whom correspondence should be addressed:
Email: jlbchamp@caltech.edu

Number of Pages: 14

Number of Figures: 6

Number of Tables: 1

**Table of Contents**

| | |
|---|---|
| Materials | S2 |
| Design of Enclosure for FIDI-MS Experiments | S2 |
| Environmental Chamber Protocol | S5 |
| Photochemical Box Model | S6 |
| Speciation of Soluble Iron (III) as a Function of pH | S11 |
| Control Experiments for Photochemistry of Iron (III) Oxalate and Glycolaldehyde | S12 |

**Additional Experimental Details**

*Materials*

High-purity water and ACS-grade sulfuric acid were obtained from EMD Millipore (Billerica, MA). Concentrated ammonium hydroxide (28-30% by weight) and ACS-grade iron (III) chloride 6-hydrate were obtained from J.T. Baker Avantor (Center Valley, PA). All other chemicals were purchased from Sigma-Aldrich (St. Louis, MO). Stock solutions of components used in studies of droplet photochemistry were prepared in concentrations of 10-100 mM and stored at −20° C with the exception of iron (III) chloride stock solutions, which were prepared fresh daily at a concentration of 50 mM in a 5 mM solution of $H_2SO_4$. The pH of samples was measured utilizing non-bleeding pH-indicator strips (MColorpHast, EMD Millipore).

*Design of Enclosure for FIDI-MS Experiments*

The FIDI-MS source utilized in this study is designed to allow for control of the ambient environment in which suspended droplet chemistry is studied. The device consists of four main parts: an enclosure, a back plate, and viewport plates, all machined by eMachineShop (Mahwah, NJ). The assembled source is shown in Figure S1a. The interface with the mounts of the LTQ mass spectrometer is based upon a design for a custom electrospray stage by Priska D. von Haller at the University of Washington Proteomics Resource. The device seals to the front of the mass spectrometer utilizing an O-ring present on the atmospheric pressure interface, normally utilized to seal the commercially available atmospheric pressure ionization sources. Once mounted, the entire device can reach a vacuum pressure of approximately 10 Torr utilizing only the draw of gas through the atmospheric pressure interface of the LTQ.

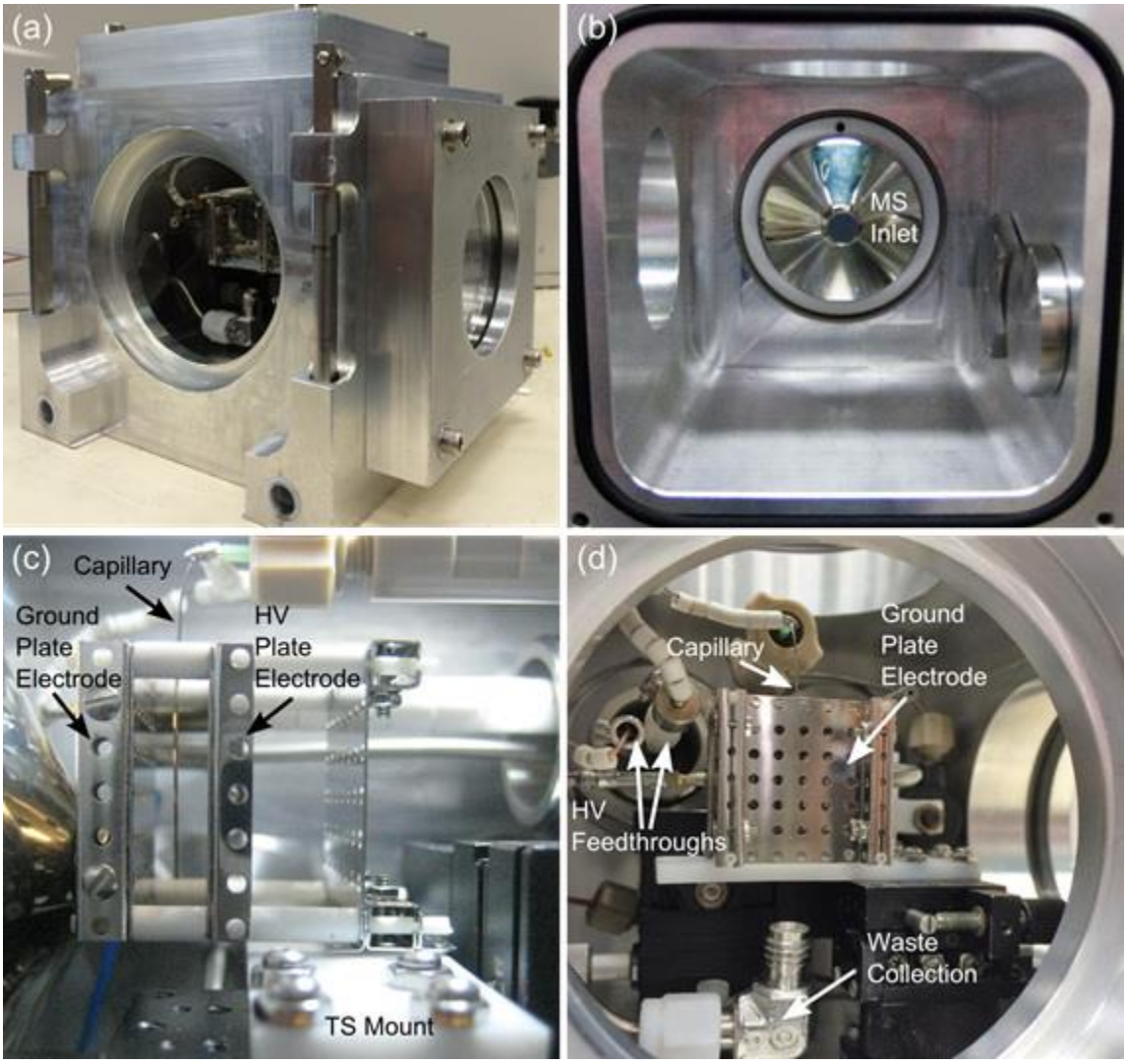


**Figure S1.** Enclosure for FIDI experiments with atmospheric control; shown in (a) is the assembled source, while the main enclosure mounted to the mass spectrometer inlet is shown in (b). Shown in (c) and (d) are two views of the FIDI apparatus mounted within the enclosure.

Shown in Figure S1b is an image of the main enclosure mounted to the inlet of the LTQ mass spectrometer. The right side of the enclosure is equipped with two 1" baseplate apertures, which allow for the mounting of various feedthrough interfaces. In this study, the apertures are mounted with 1/8" outer diameter (OD) feedthroughs (FCH-012S, Kurt J. Lesker, Jefferson, Hills, PA) to introduce liquid to the FIDI capillary and collect waste droplets from the enclosure. The backing

plate of the enclosure is also equipped with three 1" baseplate apertures and is sealed to the main enclosure by a Viton O-ring (McMaster-Carr, Santa Fe Springs, CA). The backing plate holds a gas feedthrough (LFT421TETE, Kurt J. Lesker) to control the ambient conditions in the chamber and a high voltage feedthrough (A0507-1-QF, MPF Products, Gray Court, SC) to apply an electric potential to the FIDI apparatus.

The enclosure is also equipped with glass viewport mounts on the top and left side of the device to allow for visual monitoring and to initiate photochemistry. The viewport mounts are based on a design detailed by Abbott and Scace in which the glass window is sealed on each side by compression of an O-ring, avoiding direct glass-metal contact.[1] Glass windows of 80 mm diameter and 12 mm thickness were obtained from OptoSigma (Santa Ana, CA), with the top window fabricated from BK7 glass and the side window fabricated from fused silica to allow for efficient UV transmission.

Within the enclosure, the FIDI apparatus is based upon a design described previously by Grimm and co-workers.[2] The source region is fabricated from eV parts (Kimball Physics, Wilton, NH), with the high voltage and ground plates (SS-PL-B7x7) mounted on ceramic rods (Al2O3-TU-B-2000) secured to a custom PTFE mount via a bracket (SS-BR-B2x7). The plates are held in position by a combination of screw clamps (SS-SC-B7) and ceramic spacers (AL2O3-TU-C-250). The mount is affixed to a translation stage for alignment with the inlet of the mass spectrometer. The stainless steel (SS) capillary (28 gauge, McMaster-Carr) is also connected to a translation stage by 1/16" OD stainless steel tubing (0.005" ID, Sigma-Aldrich, St. Louis, MO) for alignment between the two plates.

*Environmental Chamber Protocol*

Figure S2 illustrates the sequence of steps taken to conduct a chamber experiment. First, aerosol was injected into the chamber using a constant output atomization system operated at 35 psi. To achieve comparable aerosol loadings between experiments, the atomization process was timed for 30 minutes, and aerosol number concentrations were monitored by SMPS. Prior to entering the chamber, aerosol was passed through a custom-built wet-walled humidifier to ensure that particles were humidified above the deliquescence point for ammonium sulfate seed (~80%).[3]

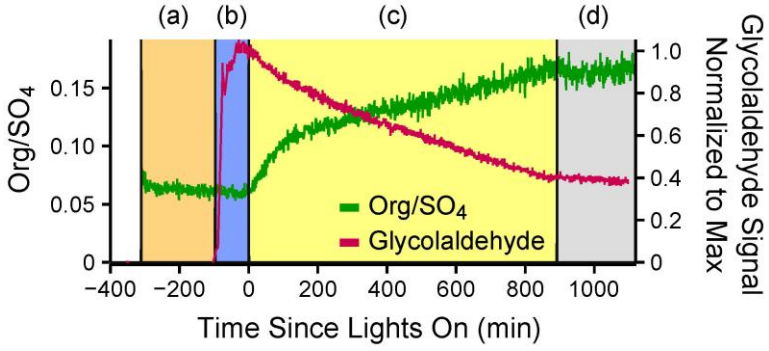


**Figure S2**. Data from Experiment 2 (AS + Gly) illustrating the typical chamber experimental procedure. The sequence of events was (a) inject aerosol and wait for HR-AMS signal to stabilize, (b) inject glycolaldehyde and wait for CIMS signal to stabilize, (c) turn on lights to induce photochemistry, and (d) turn off lights.

Glycolaldehyde was injected into the chamber by passing filtered, dry air through a bulb containing 7.5 mg of glycolaldehyde dimer. The bulb was heated to 85° C in a water bath to melt glycolaldehyde solids. The injection of glycolaldehyde was monitored by CIMS and proceeded until the concentration in the chamber reached ~ 100 ppb. The aerosol/glycolaldehyde mixture was allowed to mix for several hours and was monitored by CIMS, AMS, SMPS, and $O_3$/$NO_x$ instrumentation. After sufficient mixing, 100% of the chamber UV lights were turned on to

induce photochemistry for 24 hours. For some experiments, lights were turned off, and instruments were permitted to sample until gas and particle-phase species stabilized.

*Photochemical Box Model and Formation of Organic Aerosol During Iron-Free Experiments.*

Table S1 lists the set of reactions and initial conditions used to model glycolaldehyde photolysis. All rate constants originate from the JPL evaluation of chemical kinetics and photochemical data (jpldataeval.jpl.nasa.gov/)[4] unless otherwise noted. Photolysis rate constants were calculated using measured UV spectrum and published absorption cross-sectional data. Ozone was observed to rise over the course of an experiment to ~ 14 ppb; consequently, low levels of $NO_x$ were likely present in the Teflon chamber. The Teledyne $NO_x$ analyzers have a detection limit of 0.4 ppb. Modeling iterations were performed by changing initial $NO_2$ concentrations until modeled $O_3$ concentrations matched those from observations. Initial $NO_2$ concentrations in the chamber were estimated to be 0.13 ppb.

Figure S3 compares the box model results to measured glycolaldehyde decay and ozone formation. The model satisfactorily reproduces the observed glycolaldehyde decay to within 15%. The low levels of $NO_X$ in the bag contribute to the formation of OH radicals through the reaction of $HO_2$ with NO. If we remove $NO_X$ from the model, the decay of glycolaldehyde by strict photolysis does not adequately reproduce the observations (Fig. S3b). Consequently, ~50% of the observed glycolaldehyde decay (i.e., the difference between the $NO_X$ and no-$NO_X$ simulations) is attributable to the glycolaldehyde + OH reaction.

These results demonstrate that OH-chemistry likely affected the gas-phase loss of glycolaldehyde during seeded experiments. Magneron *et al.* estimated that glyoxal is formed by the glycolaldehyde + OH reaction at a yield of ~22%.[5] The photochemical box model predicts glyoxal production of ~ 3.5 ppb, which is consistent with the production expected based on the fraction of glycolaldehyde decay attributable to the OH + glycolaldehyde reaction.

Consequently, gas-phase organics, such as glyoxal, were likely formed during seeded experiments.

The production of glyoxal has important implications for SOA growth. Glyoxal has been previously shown to efficiently generate SOA in ammonium sulfate seed via dark reactions that lead to the formation oligomers and imines.[6-10] The observation of organic growth after the initiation of photochemistry during Experiment 2 (Table 1) suggests that secondary products significantly contributed to the formation of SOA. We hypothesize that glyoxal SOA constitutes an important fraction of this organic aerosol; however, quantification of glyoxal SOA is beyond the scope of this study.

**Table S1**. Reactions, Rate Constants, and Initial Conditions Used to Model Glycolaldehyde Photolysis (Exp. 1, Table 1).

| **Glycolaldehyde Reactions** | **Rate Constant ($molec^{-(n-1)}\ cm^{3\ (n-1)}\ s^{-1}$)** | **NOTES** |
|---|---|---|
| $Gly + hv \rightarrow 0.83(HCHO + CO + 2\ HO_2) + 0.1(CH_3OH+CO) + 0.07(OH + CH_2CHO)$ | 2.10e-06 | Magneron *et al.* (Ref. 5) |
| $Gly + OH + (O2) \rightarrow HOCH_2CO_3$ | 0.8e-11 | Branching ratio = 0.8 (Ref. 4) |
| $Gly + OH + (O2) \rightarrow Glyoxal + HO_2$ | 2.5e-12 | Branching ratio = 0.2 (Ref. 4) |
| **Glycolaldehyde Product Reactions** | **Rate Constant ($molec^{-(n-1)}\ cm^{3\ (n-1)}\ s^{-1}$)** | |
| $HCHO + OH + (O_2) \rightarrow HO_2 + CO + H_2O$ | 9.36e-12 | |
| $HCOOH + OH \rightarrow HO_2 + CO_2 + H_2O$ | 4.5e-13 | |

| | | |
|---|---|---|
| $CO + OH \rightarrow CO_2 + HO_2$ | 1.5e-13 | |
| $HCHO + hv + (O_2) \rightarrow H + CO + HO_2$ | 8.10e-06 | |
| $HCHO + hv \rightarrow H_2 + CO$ | 2.74e-05 | |
| $HCHO + HO_2 \rightarrow HOCH_2O_2$ | 5.01e-14 | |
| $HOCH_2O_2 \rightarrow HCHO + HO_2$ | 125 | |
| $HOCH_2O_2 + HO_2 \rightarrow$ Prod | 1.25e-11 | |
| $CH_3OH + OH \rightarrow HCHO + HO_2 + 0.85\ H_2O$ | 9.11e-13 | |
| $Glyx + OH + (O_2) \rightarrow H_2O + CO + CO + HO_2$ | 1.15e-11 | |
| $HOCH_2CO_3 + HO_2 \rightarrow 0.44\ (HO_2 + HCHO + OH) + 0.15$ (Glycolic Acid + $O_3$) + 0.41 (Glycolic Acid) | 1.39e-11 | Master Chemical Mechanism (Ref. 10) |
| $HOCH_2CO_3 + HOCH_2CO_3 \rightarrow 0.7*(HCHO + HO_2) + 0.3$ (2*Glycolic Acid) | 1e-11 | Master Chemical Mechanism (Ref. 10) |
| | | |
| **O1D Reactions** | **Rate Constant ($molec^{-(n-1)}\ cm^{3\ (n-1)}\ s^{-1}$)** | |
| $O1D + N_2 \rightarrow O3P + N_2$ | 2.51e-11 | |
| $O1D + O_2 \rightarrow O3P + O_2$ | 4.04e-11 | |
| $O1D + H_2O \rightarrow 2OH$ | 2e-10 | |
| $O1D + O_3 \rightarrow O_2 + O_2$ | 1.2e-10 | |
| $O1D + O_3 \rightarrow O2 + O3P + O3P$ | 1.2e-10 | |
| $O1D + H_2 \rightarrow OH + H$ | 1.2e-10 | |
| **HOx Reactions** | **Rate Constant ($molec^{-(n-1)}\ cm^{3\ (n-1)}\ s^{-1}$)** | |
| $O3P + O_2 + M \rightarrow O_3 + M$ | 6.09e-34 | |
| $O3P + O_3 \rightarrow O_2 + O_2$ | 7.96e-15 | |

| | | |
|---|---|---|
| $O3P + OH \rightarrow O_2 + H$ | 3.29e-11 | |
| $O3P + HO_2 \rightarrow OH + O_2$ | 5.87e-11 | |
| $O3P + H_2O_2 \rightarrow OH + HO_2$ | 1.70e-15 | |
| $H + O_2 + M \rightarrow HO_2$ | 4.43e-32 | |
| $OH + OH \rightarrow H_2O + O3P$ | 1.8e-12 | |
| $OH + OH + M \rightarrow H_2O_2$ | 6.94e-31 | |
| $OH + HO_2 \rightarrow H_2O + O_2$ | 1.11e-10 | |
| $HO_2 + HO_2 \rightarrow H_2O_2 + O_2$ | 2.92e-12 | |
| $O_3 + OH \rightarrow HO_2 + O_2$ | 7.25e-14 | |
| $O_3 + HO_2 \rightarrow OH + 2O_2$ | 2.12e-15 | |
| $H_2O_2 + OH \rightarrow HO_2 + H_2O$ | 1.69e-12 | |
| $H_2O_2 + hv \rightarrow OH + OH$ | 3.19e-6 | |
| $O_3 + hv \rightarrow O1D + O_2$ | 4.65e-6 | |
| **NOx Reactions** | **Rate Constant** $(molec^{-(n-1)}\ cm^{3\ (n-1)}\ s^{-1})$ | |
| $NO_2 + hv \rightarrow NO + O3P$ | 4.44e-3 | |
| $NO_3 + hv \rightarrow NO_2 + O3P$ | 2.311e-3 | |
| $NO_3 + hv \rightarrow NO + O_2$ | 3.73e-5 | |
| $HONO + hv \rightarrow NO + OH$ | 6.11e-4 | |
| $NO + OH \rightarrow HONO$ | 7.6e-12 | |
| $O_3 + NO \rightarrow NO_2 + O_2$ | 1.82e-14 | |
| $O_3 + NO_2 \rightarrow NO_3 + O_2$ | 3.22e-17 | |
| $NO + NO_3 \rightarrow 2NO_2$ | 2.65e-11 | |
| $HO_2 + NO \rightarrow NO_2 + OH$ | 8.16e-12 | |
| $HO_2 + NO_2 \rightarrow HONO + O_2$ | 5e-16 | |

| | | |
|---|---|---|
| $HO_2 + NO_3 \rightarrow OH + NO_2 + O_2$ | 3.5e-12 | |
| **Initial Conditions** | **Concentration (ppb)** | |
| Gly | 85 | |
| $NO_2$ | 0.13 | |
| All other species | 0 | |

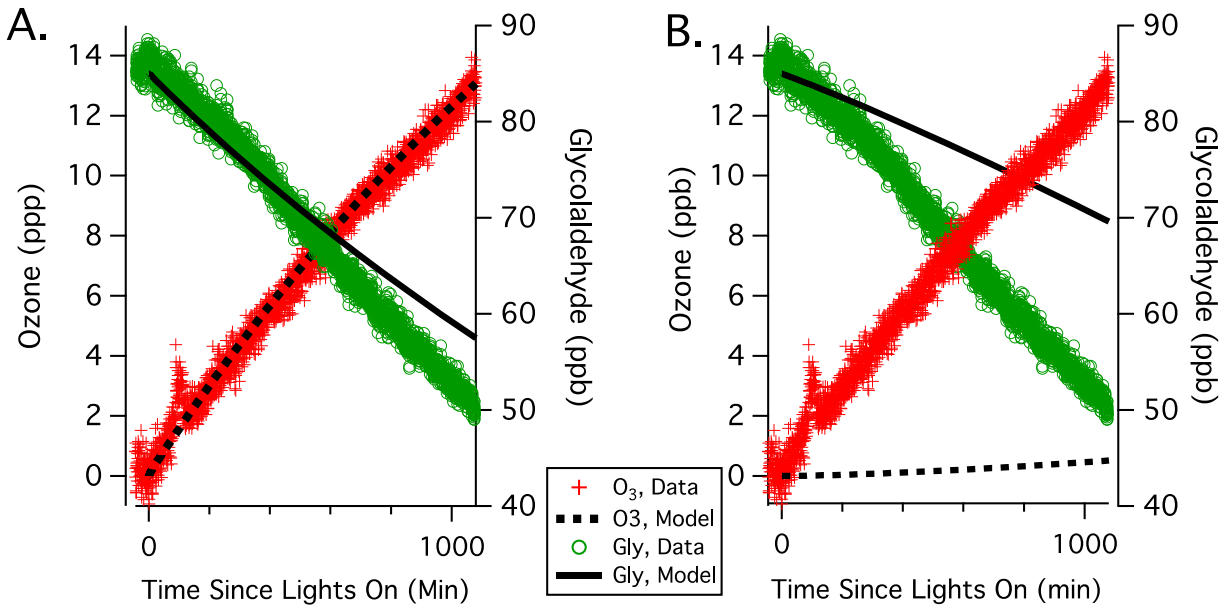


**Figure S3**. Photochemical box model results compared to the decay of glycolaldehyde and formation of ozone for (a) model assuming 0.13 ppb of $NO_X$ and (b) no $NO_X$. The presence of $NO_X$ enhances glycolaldehyde decay by ~50%. The model predicts the formation of secondary organics, such as glyoxal (~3.5 ppb).

**Speciation of Soluble Iron (III) as a Function of pH**

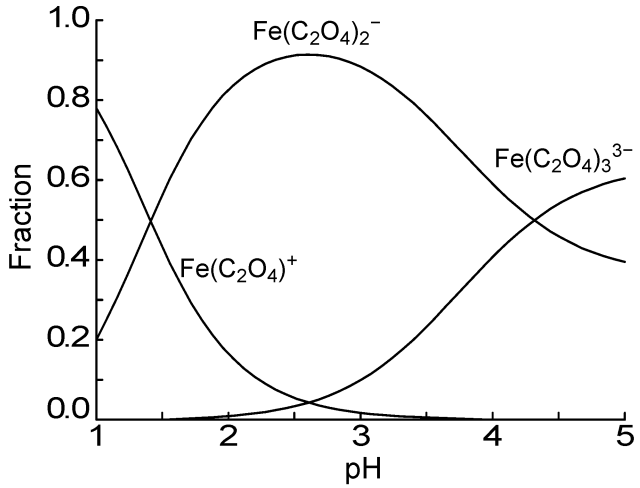


**Figure S4**. Speciation of soluble iron (III) as a function of pH under conditions utilized for FIDI-MS experiments. Solution conditions: $[Fe^{3+}]$ = 50 μM, $[Cl^-]$ = 150 μM, $[H_2C_2O_4]$ = 250 μM, $[H_2SO_4]$ = 0.5 mM, $[NH_3]$ = 100 μM. Fractions were calculated using the MEDUSA program (*MEDUSA-Make Equilibrium Diagrams Using Sophisticated Algorithms, Puigdomenech, I. Royal Institute of Technology 100 44 Stockholm, Sweden; 2010*).

**Control Experiments for Photochemistry of Iron (III) Oxalate and Glycolaldehyde**

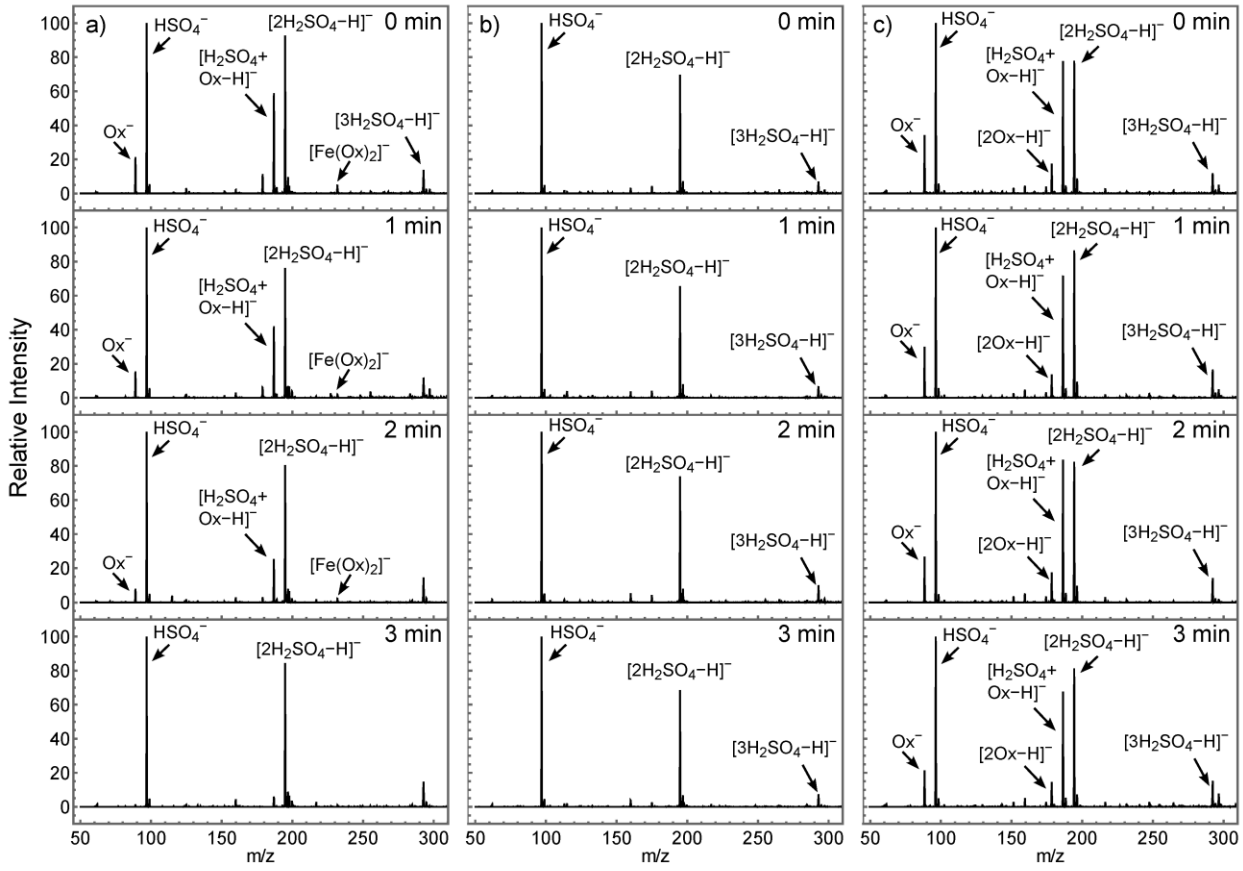


**Figure S5**. Control experiments for the oxidation of glycolaldehyde by photodissociation of iron (III) oxalate complexes; (a) iron (III) and oxalic acid only (no glycolaldehyde added), (b) iron (III) and glycolaldehyde only (no oxalic acid added), (c) glycolaldehyde and oxalic acid only (no iron added).

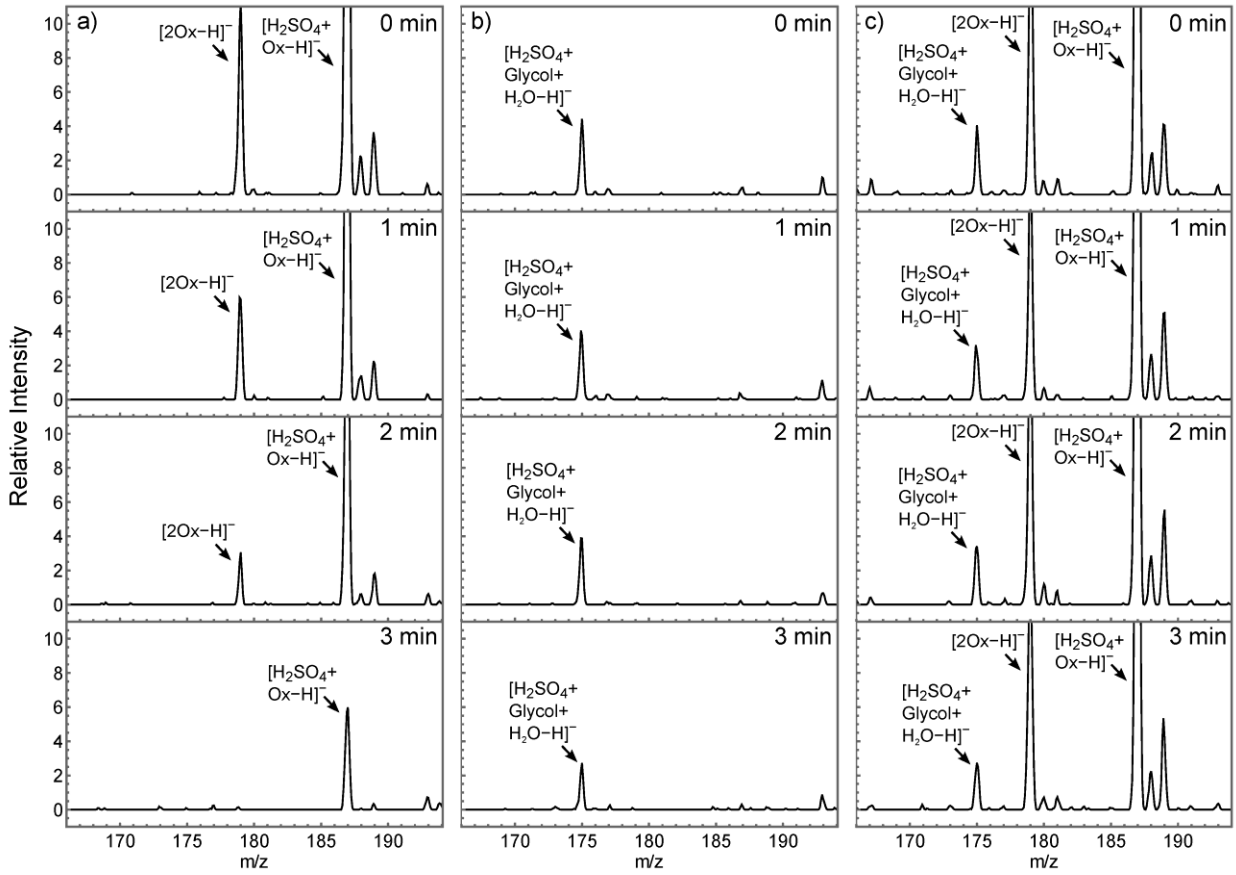


**Figure S6**. Control experiments for the oxidation of glycolaldehyde by photodissociation of iron (III) oxalate complexes, zoomed on product region; (a) iron (III) and oxalic acid only (no glycolaldehyde added), (b) iron (III) and glycolaldehyde only (no oxalic acid added), (c) glycolaldehyde and oxalic acid only (no iron added).

**References**


1. Abbott, P. J.; Scace, B., Safely mounting glass viewports to elastomer sealed vacuum flanges. *J. Vac. Sci. Technol. A* **2010,** *28*, (4), 573-577.
2. Grimm, R. L.; Hodyss, R.; Beauchamp, J. L., Probing Interfacial Chemistry of Single Droplets with Field-Induced Droplet Ionization Mass Spectrometry: Physical Adsorption of Polycyclic Aromatic Hydrocarbons and Ozonolysis of Oleic Acid and Related Compounds. *Anal. Chem.* **2006,** *78*, (11), 3800-3806.
3. Brooks, S. D.; Wise, M. E.; Cushing, M.; Tolbert, M. A., Deliquescence behavior of organic/ammonium sulfate aerosol. *Geophys. Res. Lett.* **2002,** *29*, (19), 1917.
4. Burkholder, J. B.; Sander, S. P.; Abbatt, J.; Barker, J. R.; Huie, R. E.; Kolb, C. E.; Kurylo, M. J.; Orkin, V. L.; Wilmouth, D. M.; Wine, P. H., *Chemical Kinetics and Photochemical Data for Use in Atmospheric Studies, Evaluation No. 18, JPL Pub. 15-10*. NASA Jet Propulsion Laboratory: Pasadena, CA, 2015.
5. Magneron, I.; Mellouki, A.; Le Bras, G.; Moortgat, G. K.; Horowitz, A.; Wirtz, K., Photolysis and OH-Initiated Oxidation of Glycolaldehyde under Atmospheric Conditions. *J. Phys. Chem. A* **2005,** *109*, (20), 4552-4561.
6. Galloway, M. M.; Chhabra, P. S.; Chan, A. W. H.; Surratt, J. D.; Flagan, R. C.; Seinfeld, J. H.; Keutsch, F. N., Glyoxal uptake on ammonium sulphate seed aerosol: reaction products and reversibility of uptake under dark and irradiated conditions. *Atmos. Chem. Phys.* **2009,** *9*, (10), 3331-3345.
7. Galloway, M. M.; Loza, C. L.; Chhabra, P. S.; Chan, A. W. H.; Yee, L. D.; Seinfeld, J. H.; Keutsch, F. N., Analysis of photochemical and dark glyoxal uptake: Implications for SOA formation. *Geophys. Res. Lett.* **2011,** *38*, (17), L17811.
8. Ervens, B.; Volkamer, R., Glyoxal processing by aerosol multiphase chemistry: towards a kinetic modeling framework of secondary organic aerosol formation in aqueous particles. *Atmos. Chem. Phys.* **2010,** *10*, (17), 8219-8244.
9. Kampf, C. J.; Waxman, E. M.; Slowik, J. G.; Dommen, J.; Pfaffenberger, L.; Praplan, A. P.; Prévôt, A. S. H.; Baltensperger, U.; Hoffmann, T.; Volkamer, R., Effective Henry's Law Partitioning and the Salting Constant of Glyoxal in Aerosols Containing Sulfate. *Environ. Sci. Technol.* **2013,** *47*, (9), 4236-4244.
10. Saunders, S. M.; Jenkin, M. E.; Derwent, R. G.; Pilling, M. J., Protocol for the development of the Master Chemical Mechanism, MCM v3 (Part A): tropospheric degradation of non-aromatic volatile organic compounds. *Atmos. Chem. Phys.* **2003,** *3*, (1), 161-180.